Coupling-length phase matching for nonlinear optical frequency conversion in parallel waveguides

Ivan Biaggio
Department of Physics, Lehigh University, Bethlehem, Pennsylvania 18015, USA

Virginie Coda and Germano Montemezzani
Université de Lorraine, LMOPS, EA 4423, 57070 Metz, France
and Supélec, LMOPS, EA 4423, 57070 Metz, France
(Received 2 July 2014; published 13 October 2014)

We describe and analyze a quasi-phase-matching scheme for nonlinear optical frequency conversion where the spatial modulation of mode intensity in coupled parallel waveguides provides the required modulation in the generation of the frequency conversion signal, instead of a variation of any material parameter or propagation constant. We analyze this coupling-length phase-matching (CLPM) scheme both for second-order frequency conversion, such as second harmonic generation or difference-frequency generation, as well as for third-order four-wave mixing processes, for which we consider the example of generating a longer wavelength by third-order nonlinear mixing of two shorter wavelength waves. Numerous phase-matching conditions are identified in each case. We show that the maximum photon conversion efficiencies reached after an optimum propagation length are always higher than half those obtained for perfect phase matching in a single waveguide, with nearly 100% photon conversion possible for several of the CLPM conditions we studied.

DOI: 10.1103/PhysRevA.90.043816 PACS number(s): 42.65.Ky, 42.65.Wi, 42.81.Qb, 42.79.Gn

I. INTRODUCTION

The phase-matched interaction of optical waves that is required for efficient nonlinear optical frequency conversion [1] can be achieved through a spatial modulation of the source nonlinear optical polarization responsible for radiating the generated wave. The most common implementation of such a "quasi-phase-matching" scheme involves spatial changes of the nonlinear optical response [1,2], as can be obtained, for instance, by periodically poling ferroelectric nonlinear crystals. Alternative approaches involve the modulation of the geometry of a nonlinear waveguide in order to spatially modulate the effective refractive index or the propagation constant of the interacting waves [3–6].

An interesting but less known alternative for quasi-phase-matching consists in modulating the intensities of the interacting waves with individual spatial periodicities, as proposed earlier for second harmonic generation in coupled waveguides [7–10].

Such an intensity modulation can be easily obtained if the interacting waves are made to travel along parallel waveguides that allow the light to couple from one waveguide to the other. Figure 1 shows a schematic representation of this idea. The coupling lengths between the optical modes are then responsible for an effective coupling length phase-matching (CLPM) process. The coupling constants between the waveguides play the role of "coupling wave vectors" that can compensate any mismatch between the sum of the wave vectors of the fundamental waves and that of the generated wave. In the present work we give a systematic treatment of CLPM in two coupled parallel waveguides in the absence of any modulation of linear or nonlinear optical properties. We extend previous work [7–11] by developing a general framework for CLPM, and we provide a large set of phase-matching conditions for sum-frequency generation, difference-frequency generation, and one case of frequency conversion via third-order nonlinear optical effects. The latter is particularly interesting for use in multicore fibers. In addition, we will also present an analysis of the maximum photon-conversion efficiency that can be reached after an optimum interaction length for the various possible CLPM configurations.

Below we introduce the CLPM concept starting with second-order frequency conversion. We discuss the phase-matching conditions for the interaction of three waves with different frequencies $\omega_3 > \omega_2 > \omega_1$, for application such as optical parametric generation or the generation of a new frequency from two strong pump waves. In particular, we will discuss the CLPM conditions for sum-frequency generation [(SFG) $\omega_3 = \omega_1 + \omega_2$], difference-frequency generation [(DFG) $\omega_1 = \omega_3 - \omega_2$], as well as second harmonic generation [(SHG) $\omega_3 = 2\omega_1 = 2\omega_2$] as a special case. This is then

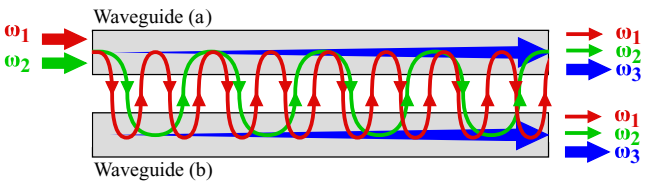

FIG. 1. (Color online) Schematic diagram of the principle of coupling-length phase-matching (CLPM). The two waveguides a and b are assumed to be identical. The pump beams (at frequency ω_1 and ω_2 in this example) are injected in waveguide a. The evanescent coupling between the two waveguides causes the power of the pump waves to oscillate between the two waveguides (schematically represented in this sketch by the two lines meandering between the two waveguides). Under the appropriate CLPM condition it is possible to arrange for the signal wave at frequency ω_3 that is created by nonlinear optical interaction of the two pump waves to grow constructively with propagation length, in both waveguides. The qualitative depiction in this figure corresponds to the case of sum-frequency generation ($\omega_3 = \omega_1 + \omega_2$) that will be presented later in Fig. 2.

followed by the derivation of the CLPM conditions for one useful case of frequency conversion based on the third-order nonlinear optical response: the generation of a longer wavelength (infrared) radiation at a frequency $\omega_1 = 2\omega_2 - \omega_3$ from two shorter wavelength (visible or near infrared) waves at frequencies ω_2 and ω_3. For each of the above CLPM processes we give analytical expressions for the growth of the amplitude of the generated wave in the undepleted pump regime. We also discuss pump depletion, the corresponding saturation regime, and the limits to the efficiency of nonlinear optical frequency conversion when using CLPM.

We use the SI system throughout this work. We define scalar complex amplitudes $E^{(\omega)}(z)$ for waves traveling in the z direction in such a way that the optical electric field is given by the real part of $E^{(\omega)}(x,y,z,t) = E^{(\omega)}(z)u^{(\omega)}(x,y)\exp[i(kz-\omega t)]$, where the normalized function $u^{(\omega)}$ describes the transversal field distribution (waveguide mode) at the frequency ω. While in the ideal case all waves propagate in the fundamental TE or TM waveguide mode, the treatment below holds also without loss of generality if one or more waves are in a higher order mode, which might be useful in some cases in order to limit the phase mismatch.

The nonlinear optical response of matter is described by second- and third-order susceptibilities [12]. As an example, given waves with amplitudes $E^{(\omega_1)}$ and $E^{(\omega_2)}$ at a certain coordinate in a nonlinear optical material, the second-order nonlinear optical polarization that radiates a sum-frequency wave has, at the same coordinate, the amplitude,

$$P_{\mathrm{NL}}^{(\omega_3)} = \epsilon_0 \chi_{\mathrm{eff}}^{(2)} E^{(\omega_1)} E^{(\omega_2)}, \tag{1}$$

where ϵ_0 is the electric constant and $\chi_{\mathrm{eff}}^{(2)}(-\omega_3,\omega_2,\omega_1)$ is the effective second-order susceptibility that depends on the polarization of the interacting waves with respect to the third-rank tensor of the second-order nonlinear optical susceptibility. For the degenerate case of second harmonic generation (SHG) one has

$$P_{\mathrm{NL}}^{(2\omega)} = \tfrac{1}{2}\epsilon_0 \chi_{\mathrm{eff}}^{(2)} [E^{(\omega)}]^2. \tag{2}$$

The third-order nonlinear optical polarization responsible for the third-order difference-frequency process we are interested in is

$$P_{\mathrm{NL}}^{(\omega_1)} = \tfrac{3}{4}\epsilon_0 \chi_{\mathrm{eff}}^{(3)} [E^{(\omega_2)}]^2 E^{(\omega_3)*}, \tag{3}$$

where the superscript asterisk stands for complex conjugation and $\chi_{\mathrm{eff}}^{(3)}(-\omega_1,\omega_2,\omega_2,-\omega_3)$ is the effective third-order susceptibility.

II. COUPLED WAVE ANALYSIS

We consider the case of three waves at frequencies ω_1, ω_2, and $\omega_3 = \omega_1 + \omega_2$ interacting with each other via the second-order nonlinear optical susceptibility. The interaction occurs within two waveguides that are identical and parallel to each other. We describe waveguide modes with complex amplitudes $E^{(a,\omega_i)}(z)$ and $E^{(b,\omega_i)}(z)$ that propagate in waveguide a and waveguide b and can couple from one waveguide to the other. We also introduce the amplitudes

$$A_i^{(a,b)}(z) = \sqrt{\frac{n_i}{\omega_i}} E^{(a,b,\omega_i)}(z), \tag{4}$$

where n_i is the effective refractive index for a wave with frequency ω_i. These amplitudes are proportional to the square root of the photon flux in waveguides a and b, respectively. Later we will present graphs of the evolution of these amplitudes as the interacting waves propagate, which will allow one to directly visualize the photon flux and to easily evaluate conversion efficiencies based on photon numbers. This is useful because such photon conversion efficiencies are independent of the specific frequencies ω_1, ω_2, and ω_3 of the three interacting waves.

The three coupled wave equations for the evolution of the mode amplitudes in waveguide a, expressed in terms of the amplitudes $A_i^{(a)}$ and $A_i^{(b)}$, are

$$\frac{\partial}{\partial z} A_3^{(a)} = i d A_1^{(a)} A_2^{(a)} e^{-i\Delta k\, z} + i\kappa_3 A_3^{(b)}, \tag{5}$$

$$\frac{\partial}{\partial z} A_2^{(a)} = i d A_3^{(a)} A_1^{(a)*} e^{i\Delta k\, z} + i\kappa_2 A_2^{(b)}, \tag{6}$$

$$\frac{\partial}{\partial z} A_1^{(a)} = i d A_3^{(a)} A_2^{(a)*} e^{i\Delta k\, z} + i\kappa_1 A_1^{(b)}. \tag{7}$$

Three equivalent equations hold for waveguide b. They can be obtained by permuting the superscripts (a) and (b) in each of the above equations. Here, $\Delta k = k_3 - k_2 - k_1$ is the wave-vector mismatch of the longitudinal propagation constants of the modes at the three wavelengths. The quantities $\kappa_i = \kappa(\omega_i)$ are constants describing the coupling of the given wave between the two waveguides [13]. We do not allow the κ_i to depend on the wave amplitudes, a possible higher order correction that we neglect in the present work. In the above equations, the effective nonlinear optical coupling constant between the interacting waves is given by

$$d = \frac{\chi_{\mathrm{eff}}^{(2)}}{c}\sqrt{\frac{\omega_1\omega_2\omega_3}{n_1 n_2 n_3}}\, S, \tag{8}$$

and depends on the effective nonlinear optical susceptibility $\chi_{\mathrm{eff}}^{(2)}$ introduced above and on the overlap integral S between the waveguide modes for each frequency,

$$S = \iint_{-\infty}^{+\infty} u^{(\omega_1)}(x,y) u^{(\omega_2)}(x,y) u^{(\omega_3)}(x,y) f(x,y)\, dx\, dy, \tag{9}$$

where $f(x,y)$ is a function that describes the region where the nonlinearity is active ($|f(x,y)| \leqslant 1$) and the $u^{(\omega_i)}(x,y)$ describe the transverse mode profile of the interacting waves. We recall that the degenerate limit of Eqs. (5)–(7) that corresponds to second harmonic generation is obtained by substituting $\omega_1 = \omega_2 = \omega$ and $\omega_3 = 2\omega$ in the coupled-wave equations while at the same time using a nonlinear optical constant $d/2$, i.e., half that obtained by doing the same substitution in (8). This corresponds to the degeneracy factor of one-half that must appear in (2) when there is only one distinguishable input wave for SHG.

A. Sum-frequency generation

The case of sum-frequency generation is obtained when wave 3 has zero amplitude for $z = 0$ and energy is transferred to it from the two other waves. We find an analytical solution under the "undepleted pump approximation," where we assume that the conversion efficiency remains small, so

that the two "pump" waves are not depleted by the nonlinear optical interaction. We also assume that the two pump waves, with amplitudes $A_{1,0}$ and $A_{2,0}$, are both injected in waveguide a at $z = 0$, as shown in Fig. 1. This corresponds to the easiest and most likely practical experimental implementation. Injection of both waves in both waveguides is possible in principle, but this would require one to control the relative phase of the injected waves at each wavelength because the overall effect will depend on this phase. Under the above conditions, Eqs. (6) and (7) for the two pump waves can be solved in a straightforward way to obtain $A_i^{(a)}(z) = A_{i,0}\cos(\kappa_i z)$ and $A_i^{(b)}(z) = iA_{i,0}\sin(\kappa_i z)$ $(i = 1,2)$. Inserting these expressions into (5) for each waveguide leads to the coupled equations that describe the amplitude $A_3(z)$ in waveguides a and b. Conversion of trigonometric functions to exponential notation delivers

$$\frac{\partial}{\partial z}A_3^{(a)} = \frac{id}{4}[e^{i(\kappa_1+\kappa_2)z} + e^{i(\kappa_1-\kappa_2)z} + e^{-i(\kappa_1-\kappa_2)z} + e^{-i(\kappa_1+\kappa_2)z}]e^{-i\Delta kz}A_{1,0}A_{2,0} + i\kappa_3 A_3^{(b)}, \quad (10)$$

$$\frac{\partial}{\partial z}A_3^{(b)} = \frac{id}{4}[e^{i(\kappa_1+\kappa_2)z} - e^{i(\kappa_1-\kappa_2)z} - e^{-i(\kappa_1-\kappa_2)z} + e^{-i(\kappa_1+\kappa_2)z}]e^{-i\Delta kz}A_{1,0}A_{2,0} + i\kappa_3 A_3^{(a)}. \quad (11)$$

These equations can be solved by taking the derivative with respect to z of the first equation, and substituting the second equation to obtain an equation for $A_3^{(a)}(z)$ that contains a sum over several exponential factors, multiplied by different linear combinations of the coupling constants and Δk. After some lengthy algebra one obtains an analytical expression for the amplitude of the sum-frequency wave in waveguide a that can be written as

$$A_3^{(a)}(z) = \frac{d}{4}A_{1,0}A_{2,0}\,\xi_{\mathrm{SF}}(z). \quad (12)$$

This can be rewritten in terms of the electric fields by substituting (4) and (8), to obtain

$$E^{(a,\omega_3)}(z) = \frac{\chi^{(2)}_{\mathrm{eff}}\,S\,\omega_3}{4cn_3}E_0^{(a,\omega_1)}E_0^{(a,\omega_2)}\,\xi_{\mathrm{SF}}(z). \quad (13)$$

The complex function $\xi_{\mathrm{SF}}(z)$ describes the growth with propagation length of the generated sum-frequency wave and is given by

$$\xi_{\mathrm{SF}}(z) = \frac{2(\kappa_3-\Delta k)e^{-i\kappa_3 z}}{K_1K_3} - \frac{2(\kappa_3+\Delta k)e^{i\kappa_3 z}}{K_2K_4} + \frac{e^{-i(\kappa_3-K_1)z}}{K_1} + \frac{e^{i(\kappa_3+K_2)z}}{K_2} - \frac{e^{-i(\kappa_3+K_3)z}}{K_3} - \frac{e^{i(\kappa_3-K_4)z}}{K_4}, \quad (14)$$

with

$$K_1 = \kappa_1 - \kappa_2 + \kappa_3 - \Delta k, \quad (15)$$

$$K_2 = \kappa_1 + \kappa_2 - \kappa_3 - \Delta k, \quad (16)$$

$$K_3 = \kappa_1 - \kappa_2 - \kappa_3 + \Delta k, \quad (17)$$

$$K_4 = \kappa_1 + \kappa_2 + \kappa_3 + \Delta k. \quad (18)$$

Equation (14) has several interesting properties. The first thing to note is that it is a sum of six terms with different oscillatory behavior. In general, such a sum will not lead to a constructive buildup of $A_3^{(a)}(z)$ for growing z. This is the normal case in a non-phase-matched situation. However, when one of the constants K_i $(i = 1,\ldots,4)$ approaches zero, then (for general values of the coupling constants) exactly two of the six terms in (14) diverge, dominating over the others. Interestingly, their divergence is such that their sum always remains finite at finite distances. The result of taking the limit of one $K_i \to 0$ for large z is that the other four terms remain bounded while the sum of the two diverging terms grows linearly with z. The conditions $K_i = 0$ $(i = 1,\ldots,4)$ give therefore four coupling-length phase-matching (CLPM) conditions that for a general choice of coupling constants always result, for large propagation distances, in $A_3^{(a)}(z) \to izdA_{1,0}A_{2,0}\exp(\pm i\kappa_3 z)/4$, where the negative sign in the exponent belongs to $K_1 = 0$ and $K_3 = 0$, and the positive sign belongs to $K_2 = 0$ and $K_4 = 0$ (these four CLPM conditions are listed in the first four rows of Table I). An example of a SFG process is shown in Fig. 2, which plots the growth of the sum-frequency signal for the case where the CLPM

TABLE I. CLPM Conditions for SFG and DFG in two coupled waveguides. The CLPM column lists which of the K_i verify the $K_i = 0$ condition and the resulting phase-matching conditions are summarized in the following column. The initial growth in the undepleted regime of the sum-frequency (difference-frequency) amplitude of the wave at ω_3 (ω_1) in the limit where $z \to \infty$ is given by Eq. (13) [Eq. (19)], with the factor $\xi_{\mathrm{SF}}(z)$ of Eq. (14) [$\xi_{\mathrm{DF}}(z)$ of Eq. (20)] tending to the propagation distance z multiplied by the values given in the third and fifth columns. The quantities $\eta^{\mathrm{SF}}_{\mathrm{max}}$ and $\eta^{\mathrm{DF}}_{\mathrm{max}}$ give the maximum photon-conversion efficiencies in the depleted regime for each CLPM condition. Condition 9 corresponds to conventional phase matching in a single waveguide ($\Delta k = 0$).

	CLPM rule	Effective condition	$\lim_{z\to\infty}(\xi_{\mathrm{SF}}/z)$	$\eta^{\mathrm{SF}}_{\mathrm{max}}(\%)$	$\lim_{z\to\infty}(\xi_{\mathrm{DF}}/z)$	$\eta^{\mathrm{DF}}_{\mathrm{max}}(\%)$
1	$K_1 = 0$	$\Delta k = +\kappa_1 - \kappa_2 + \kappa_3$	$ie^{-i\kappa_3 z}$	~50	$ie^{-i\kappa_1 z}$	~50
2	$K_2 = 0$	$\Delta k = +\kappa_1 + \kappa_2 - \kappa_3$	$ie^{i\kappa_3 z}$	~50	$ie^{-i\kappa_1 z}$	~50
3	$K_3 = 0$	$\Delta k = -\kappa_1 + \kappa_2 + \kappa_3$	$ie^{-i\kappa_3 z}$	~50	$ie^{i\kappa_1 z}$	~50
4	$K_4 = 0$	$\Delta k = -\kappa_1 - \kappa_2 - \kappa_3$	$ie^{i\kappa_3 z}$	~50	$ie^{i\kappa_1 z}$	~50
5	$K_1 = K_2 = 0$	$\Delta k = \kappa_1, \kappa_2 = \kappa_3$	$2i\cos(\kappa_3 z)$	~50	$2ie^{-i\kappa_1 z}$	~100
6	$K_1 = K_3 = 0$	$\Delta k = \kappa_3, \kappa_1 = \kappa_2$	$2ie^{-i\kappa_3 z}$	~100	$2i\cos(\kappa_1 z)$	~50
7	$K_2 = K_3 = 0$	$\Delta k = \kappa_2, \kappa_1 = \kappa_3$	$2i\cos(\kappa_3 z)$	~50	$2i\cos(\kappa_1 z)$	~100
8	$K_1 = K_2 = K_3 = 0$	$\Delta k = \kappa_1 = \kappa_2 = \kappa_3$	$3i\cos(\kappa_3 z) + \sin(\kappa_3 z)$	~86	$3i\cos(\kappa_1 z) + \sin(\kappa_1 z)$	~98
9	$K_1 = K_2 = K_3 = K_4 = 0$	$\Delta k = \kappa_1 = \kappa_2 = \kappa_3 = 0$	$4i$	100	$4i$	100

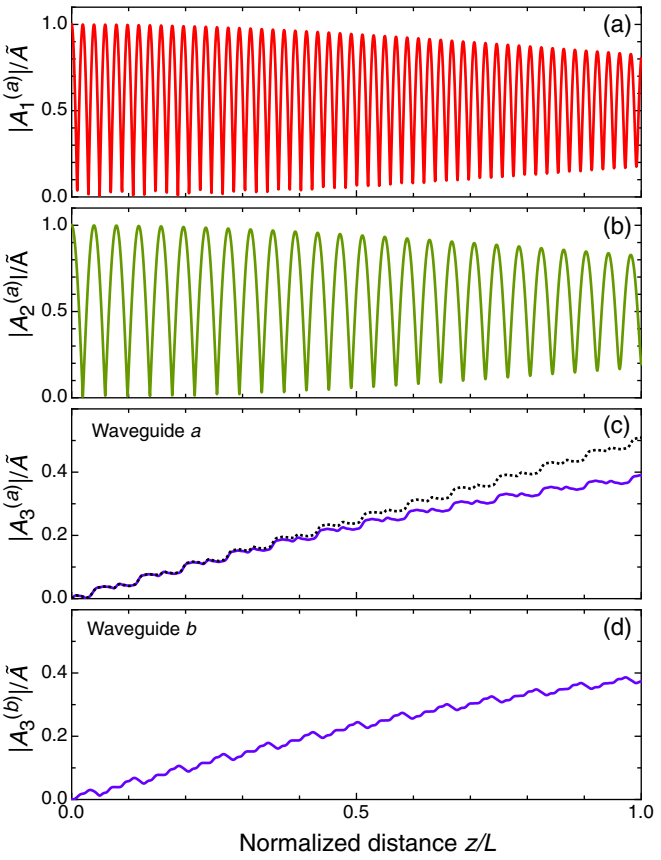

FIG. 2. (Color online) Spatial evolution of the absolute values of the wave amplitudes in the case of SFG under the CLPM condition $K_2 = 0$ in parallel waveguides of length L. All solid curves are obtained in the pump depletion regime by a numerical solution of Eqs. (5)–(7) and the corresponding equations for waveguide b. Panels (a) and (b) give the amplitudes, in waveguide a, of the pump waves at frequency ω_1 and ω_2, respectively. The generated sum-frequency wave amplitude is shown for both waveguides in (c) and (d), respectively. The amplitudes are normalized to $\tilde{A} = |A_{1,0}^{(a)} A_{2,0}^{(a)}|^{1/2}$ and the nonlinearity constant used for the plots is given by $Ld = 2/\tilde{A}$, with L the length of the waveguide. The other parameters are $\kappa_1 L = 160$, $\kappa_2 L = 80$, $\kappa_3 L = 40$, and $\Delta k L = 200$. The nondepleted analytical solution (12) corresponds to the initial part at short distances and is given explicitly in (c) as a dotted black curve.

condition $K_2 = \kappa_1 + \kappa_2 - \kappa_3 - \Delta k = 0$ is valid. The curves are obtained in the pump depletion regime by numerically solving Eqs. (5)–(7) together with the corresponding equations for waveguide b. The initial linear growth of the envelope of the wave at frequency ω_3 seen in Figs. 2(c) and 2(d) reflects the analytical solution (13) valid in the undepleted pump regime. It can be seen that this analytical solution describes the conversion process very well in the weak conversion regime. As a rule of thumb, a departure from the analytic behavior approximately takes place for propagation distances exceeding the point where roughly 20% of the maximum convertible photons have been frequency converted. This is true for most CLPM configurations discussed in this work. We note also that in the case depicted in Fig. 2 both waveguides carry essentially the same sum-frequency intensity. This is no longer the case for some other interesting CLPM conditions that we will discuss later.

In summary, for a general choice of coupling constants a CLPM condition $K_i = 0$ causes two of the six terms in (14) to become dominant and to combine constructively to give a signal wave intensity that grows quadratically with distance. The effective nonlinearity that describes this growth in each waveguide is $\chi_{\rm eff}^{(2)}/4$, which is smaller than the $2\chi_{\rm eff}^{(2)}/\pi$ one gets for conventional quasi-phase-matching in a single waveguide through the periodic inversion of the sign of the nonlinearity. However, as seen in Figs. 2(c) and 2(d), in the above CLPM cases both waveguides carry the same power, and therefore the total sum-frequency power has to be multiplied by two, as discussed in more detail later.

Table I gives the various CLPM cases that are obtained under the condition that all coupling constants κ_i between the two waveguides are positive. For each case, we give the limiting value at large z for the complex amplitude of the signal wave. The four simplest phase-matching conditions discussed above correspond to lines 1–4 in Table I. It must be noted that these conditions remain valid if one or two of the coupling constants κ_i vanish. For instance, the condition in line 2 keeps its validity if $\Delta k = \kappa_1 + \kappa_2$ and $\kappa_3 = 0$, which gives $\lim_{z\to\infty}(\xi_{\rm SF}/z) = i$ and $\lim_{z\to\infty}(\xi_{\rm DF}/z) = ie^{-i\kappa_1 z}$. The latter limit will be discussed below in connection with the case of difference-frequency generation.

Since evanescent coupling is expected to be stronger at the longer than at the shorter wavelengths, one may expect in general that $\kappa_3 < \kappa_2 < \kappa_1$. Among the CLPM conditions 1–4, the second one ($K_2 = 0$) appears therefore as the easier to implement because the coupling constants κ_1 and κ_2 sum up with the same sign to compensate for larger Δk's. The CLPM condition 4 is interesting when Δk is negative, which may be the case for nonlinear processes involving polarization conversion.

We now discuss the effect of having more than one vanishing constant K_i in (14). The corresponding CLPM conditions are given in rows 5–8 of Table I. In these cases more than two of the six terms in (14) become resonant and the solution for $A_3^{(a)}(z)$ can display additional interesting behaviors. As an example, the interference between terms with different exponential factors in (14) can lead to a signal amplitude that, while still growing linearly with distance, is accompanied by rapid oscillation of the intensity between the two waveguides. This is, for example, the case when $\kappa_2 = \kappa_3$, which for $\kappa_1 = \Delta k$ leads to both $K_1 = 0$ and $K_2 = 0$ (row 5 in Table I), and to the interference of four terms in (14). As shown in Fig. 3, this results in an amplitude of the growing sum-frequency wave that is modulated by an oscillatory term $2\cos(\kappa_3 z)$. This is completely different from the case depicted in Fig. 2, where the generated wave grew hand-in-hand in both waveguides. In contrast, for the case of Fig. 3, the generated wave intensity oscillates between the two waveguides, synchronously with the pump wave at ω_2. The same result is obtained in the symmetric case where $\kappa_1 = \kappa_3$ and $\kappa_2 = \Delta k$ (row 7). On the other hand, the choice $\kappa_1 = \kappa_2$ and $\kappa_3 = \Delta k$, which corresponds to $K_1 = 0$ and $K_3 = 0$ (row 6), leads to constructive interference of three terms in (14) that all oscillate in phase, and generates a SFG amplitude

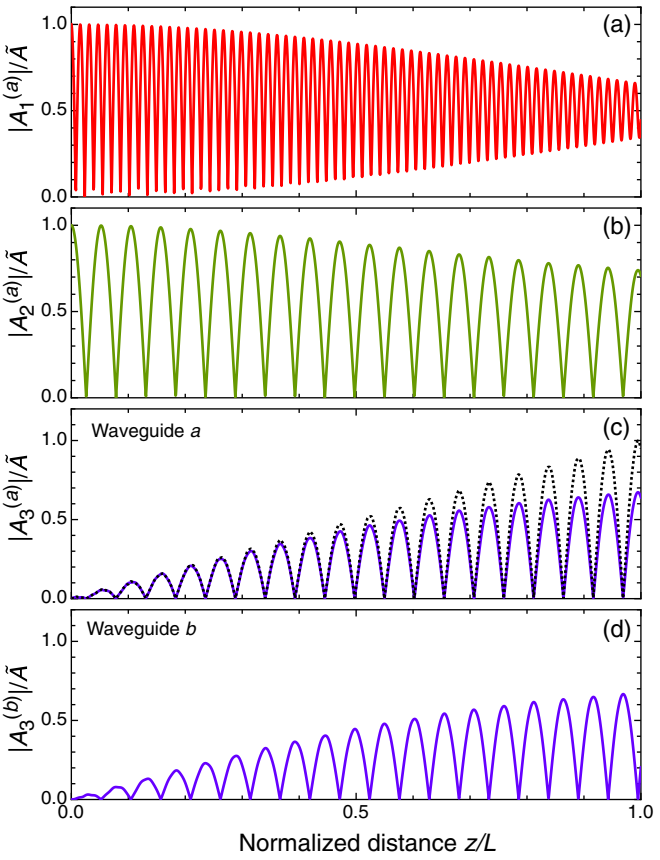

FIG. 3. (Color online) Spatial evolution of the absolute values of the SFG wave amplitudes under the CLPM condition $K_1 = K_2 = 0$ (row 5 in Table I) in parallel waveguides of length L. The curves are obtained as in Fig. 2 and for the same nonlinearity. Panels (a) and (b) give the amplitudes, in waveguide a, of the pump waves at frequency ω_1 and ω_2, respectively. The generated sum-frequency wave amplitude is shown for both waveguides in (c) and (d), respectively. The solid curves are all in the pump depletion regime. The black dotted curve in (c) corresponds to the analytic undepleted regime according to (12) and (14). For these plots $\tilde{A} = |A^{(a)}_{1,0} A^{(a)}_{2,0}|^{1/2}$, $\Delta k L = \kappa_1 L = 200$, $\kappa_2 L = \kappa_3 L = 60$, and $L d \tilde{A} = 2$.

that grows as $A^{(a)}_3(z) = z d A_1 A_2 \exp(-i\kappa_3 z)/2$. It is interesting to note that in this last case it is the two pump waves that have the same coupling constants and oscillate synchronously between the two waveguides. Because of this, both pump waves keep oscillating between the two waveguides while they are depleted in amplitude and create sum-frequency waves that grow hand-in-hand in both waveguides, a process that can go on until both pump waves are almost depleted to zero and almost complete 100% conversion of the fundamental photons to the sum-frequency wave is reached. This is the same behavior observed for the case of SHG, where the best CLPM phase-matching condition will be discussed below (first row of Table II). In contrast, for the case of row 5 in Table I (depicted in Fig. 3), the two pump waves have different coupling constants, their oscillation between the two waveguides is not synchronized, and the maximum photon conversion efficiency is limited to 50% (fourth column of Table I). Please see later for a further discussion of photon-conversion efficiencies.

For completeness, Table I lists all possible CLPM situations, including those that may at first sight seem impossible to realize because they require several coupling constants to be equal to each other. However, one can envisage devices where the oscillation of two of the interacting waves between the two waveguides remains essentially synchronized over the available length of the waveguides, which would then correspond to an effective $\kappa_i = \kappa_j$ situation. Also, the derived cases with an extra condition $\kappa_i = 0$ for one or more of the coupling constants can be experimentally approximated if the length of the waveguides is less than the corresponding coupling length. We note that the CLPM condition listed in line 8 of Table I corresponds to a fully degenerate case and we do not expect it to ever become important in practice. It gives rise to an oscillatory phenomenon where the sum-frequency amplitude in a waveguide still grows linearly with propagation distance z but rapidly oscillates (with spatial frequency $2\kappa_3$) by $\pm 50\%$ around its growing mean value. Finally, it has to be noted that the last condition in row 9 of Table I, even though it arises naturally from our formalism, is not a CLPM condition in the strict sense. It corresponds to the limiting case of perfect conventional phase matching in a single waveguide, with no coupling to the other waveguide for any of the interacting waves.

B. Second harmonic generation

Second harmonic generation corresponds to the limit of sum-frequency generation for $\omega_1 = \omega_2$ and $\kappa_1 = \kappa_2$ with the effective nonlinear optical coupling constant (8) reduced by a factor of two to take into account degeneracy factors. In this limit $K_1 = -K_3 = \kappa_3 - \Delta k$ and (14) becomes the sum of five terms. The number of CLPM conditions is reduced, and those that remain are listed in Table II. We first note that the CLPM condition in line 2 has the same form as the usual quasi-phase-matching condition with the coupling constants playing the role of wave vectors. Nevertheless, the most interesting condition is the one in the first row of the table, which is valid for all values of $\kappa_1 \neq \kappa_3$ and requires tuning of only the coupling constant for the generated wave. The corresponding growth of the second harmonic wave amplitude is illustrated in Fig. 4 for two different values of κ_1, which only influences the small spatially transient oscillations but not the general slope. The CLPM condition in the first row leads to the most efficient frequency conversion scheme. In this case the effective nonlinearity that describes the second harmonic growth is $\chi^{(3)}_{\text{eff}}/2$. This is the same value obtained for bulk quasi-phase-matching when assuming a sinusoidally modulated nonlinearity and leads to a signal intensity four times larger than any other CLPM conditions with nonoscillatory growth of the second harmonic wave. It is interesting to note that, in the present case, the second harmonic field amplitude at the output of each waveguide is half the one that one would have for perfect phase matching in a single waveguide of equal length, and therefore the intensity is four times less. However, the waves out of the two waveguides, each with an amplitude $A = A^{(a)} = A^{(b)}$ can be coherently combined into a single mode with amplitude $(A^{(a)} + A^{(b)})/\sqrt{2}$, for instance, by an inverse Y junction (half Mach-Zehnder). In this way one can ultimately obtain an intensity in a single coherent output beam that is equal to the sum of the intensities

TABLE II. CLPM conditions for SHG in two coupled waveguides. Lines are numbered in the same way as for Table I to allow for easy comparison. The last column gives the maximum photon-conversion efficiency $\eta_{\max}^{\mathrm{SH}}$ in the depleted regime.

	CLPM rule	Effective condition	$\lim_{z\to\infty}(\xi_{\mathrm{SF}}/z)$	$\eta_{\max}^{\mathrm{SH}}(\%)$
1,3,6	$K_1 = K_3 = 0$	$\Delta k = \kappa_3$	$2ie^{-i\kappa_3 z}$	~100
2	$K_2 = 0$	$\Delta k = 2\kappa_1 - \kappa_3$	$ie^{i\kappa_3 z}$	~50
4	$K_4 = 0$	$\Delta k = -2\kappa_1 - \kappa_3$	$ie^{i\kappa_3 z}$	~50
2′,4′	K_2 or $K_4 = 0, \kappa_3 = 0$	$\Delta k = \pm 2\kappa_1, \kappa_3 = 0$	i	~50
5,7,8	$K_1 = K_2 = K_3 = 0$	$\Delta k = \kappa_1 = \kappa_3$	$3i\cos(\kappa_3 z) + \sin(\kappa_3 z)$	~86

in the two waveguides. The total SHG power is then given by an effective nonlinearity that is one-half that achieved for exact phase matching. This is better than the factor $4/\pi^2 \approx 0.41$ achievable by conventional quasi-phase-matching using a periodical square-wave modulation of the nonlinearity. The possibility of coherently combining the modes in the two waveguides exists for all CLPM scenarios discussed in this work and would be useful for all cases where the generated waves grow in both waveguides. As an example, coherent combination of the generated modes could be employed for the case depicted in Fig. 2—where the generated waves grows hand-in-hand in both waveguides—while it would be unnecessary for the case shown in in Fig. 3—where the generated wave oscillates between the two waveguides and can thus be fully accessed at the end of one of the two waveguides.

Going back to Table II, we would like to mention that the conditions 2′ and 4′ of the fourth row are not pure CLPM conditions, since they have been expanded by the additional rule requiring $\kappa_3 = 0$. We have added them explicitly here since this case can be easily understood in terms of conventional quasi-phase-matching where the second harmonic wave stays in one waveguide while the nonlinear polarization that generates it is modulated by the fundamental wave oscillating between the two waveguides. It is a less interesting case than the one discussed above because it is only valid when the second harmonic has zero coupling between the waveguides, which may be too stringent a requirement. As soon as there is some coupling of the second harmonic wave, then this condition goes over smoothly to the condition in line 2 that we already discussed above. The CLPM condition in row 4 would be interesting in case of anomalous dispersion or birefringence such that $\Delta k < 0$, corresponding to the case where the effective refractive index for the second harmonic wave is smaller than that for the fundamental wave. The last line in the table is the degenerate case. As for SFG, this case leads to a strong spatial oscillation in the generated signal wave.

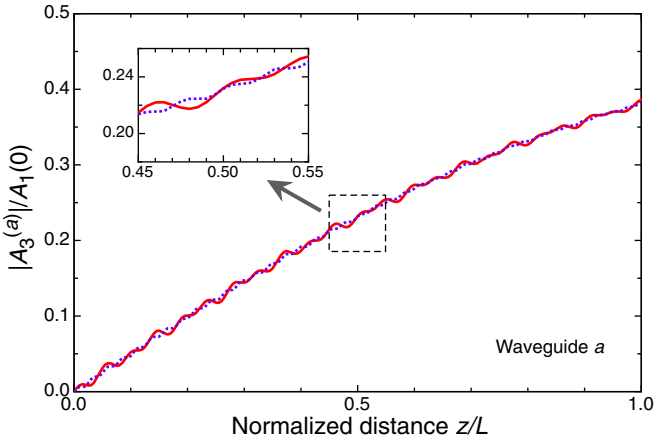

FIG. 4. (Color online) Growth of the second-harmonic signal amplitude for the optimum CLPM condition (first line of Table II) and for the same effective nonlinearity ($Ld = 2/|A_{1,0}^{(a)}|$) as in Figs. 2 and 3. Both curves are for $\Delta kL = \kappa_3 L = 40$; the solid red curve is for $\kappa_1 L (= \kappa_2 L) = 120$, and the dotted blue curve is for $\kappa_1 L = 70$. The general growth behavior is independent of κ_1, which only affects the small oscillations shown enlarged in the inset.

C. Difference-frequency generation

We now consider the case of difference-frequency generation (DFG), where a wave is generated with a frequency corresponding to the difference of the frequencies of two interacting waves. In this case the coupled wave equations are the same as Eqs. (5)–(7) but the initial condition is different. We now start with the two waves ω_3 and ω_2 injected in one waveguide, and solve for the z dependence of the wave at the lower frequency $\omega_1 = \omega_3 - \omega_2$, which initially has zero amplitude, in the undepleted pump approximation. Following the same procedure described above for SFG one finds

$$E^{(a,\omega_1)}(z) = \frac{\chi_{\mathrm{eff}}^{(2)}\omega_1}{4cn_1} E_0^{(a,\omega_3)}\left[E_0^{(a,\omega_2)}\right]^* \xi_{\mathrm{DF}}(z), \tag{19}$$

where

$$\xi_{\mathrm{DF}}(z) = -\frac{2(\kappa_1 - \Delta k)e^{-i\kappa_1 z}}{K_1 K_2} + \frac{2(\kappa_1 + \Delta k)e^{i\kappa_1 z}}{K_3 K_4} + \frac{e^{-i(\kappa_1 - K_1)z}}{K_1} + \frac{e^{-i(\kappa_1 - K_2)z}}{K_2} - \frac{e^{i(\kappa_1 - K_3)z}}{K_3} - \frac{e^{i(\kappa_1 - K_4)z}}{K_4}. \tag{20}$$

The values assumed by ξ_{DF} for the CLPM conditions in the case of DFG are listed in the second-to-last column of Table I. Note that in the SFG case the generated wave oscillates fully between the two waveguides for line 5 but not for line 6, while it is the other way around for DFG. This is because we have chosen the wave at ω_1 as the generated wave for DFG. Again, the condition in line 2 ($K_2 = 0$) appears as the easiest to implement. Condition 5 leads to an optimum conversion but might be achievable only if the wavelengths ω_3 and ω_2 are fairly close to each other. The corresponding evolution of the normalized wave amplitudes is illustrated in Fig. 5. It is evident that in this case essentially all the photons at the frequency ω_3 can be ultimately converted to

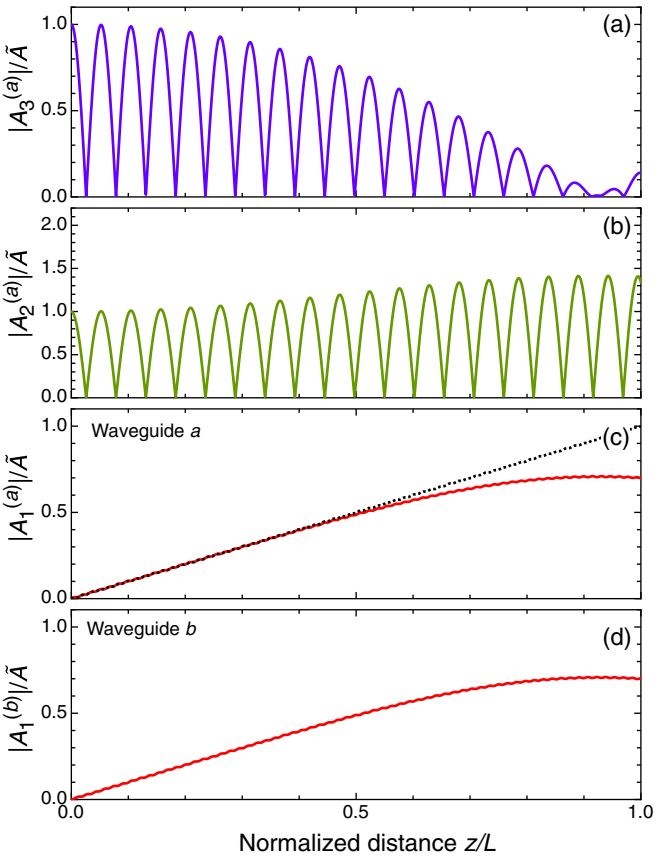

FIG. 5. (Color online) Spatial evolution of the absolute values of the DFG wave amplitudes under the CLPM condition $K_1 = K_2 = 0$ (row 5 in Table I) in parallel waveguides of length L. The curves are obtained as in Fig. 2 and for the same nonlinearity. Panels (a) and (b) give the amplitudes, in waveguide a, of the pump waves at frequency ω_3 and ω_2, respectively. The amplitude of the generated difference-frequency wave is shown for both waveguides in (c) and (d), respectively. The solid curves are all in the pump depletion regime. The black dotted curve in (c) corresponds to the analytical solution in the undepleted regime according to Eqs. (19) and (20). For these plots $\tilde{A} \equiv |A_{3,0}^{(a)} A_{2,0}^{(a)}|^{1/2}$, $\Delta k L = \kappa_1 L = 200$, $\kappa_2 L = \kappa_3 L = 60$, and $L d\tilde{A} = 2$.

photons at frequency ω_1, distributed equally between the two waveguides, which leads to a maximum photon-conversion efficiency of ∼100% (see the discussion of conversion efficiency later in this article). The undepleted solution given by (19) and (20) is still satisfactory up to about half the distance at which full depletion of the pump occurs.

We conclude this discussion of second-order effects by noting that, while we have only explicitly treated the cases of SFG and DFG, the CLPM conditions in Table I are valid in general for any second-order three-wave interaction, and they can also be used to realize phase-matched optical parametric generation or optical parametric amplification in two coupled waveguides.

D. Frequency down-conversion by third-order nonlinear optics

We now analyze the use of a third-order nonlinear optical material to generate a longer wavelength wave by the third-order interaction of two waves with shorter wavelengths. Here, two waves at frequencies $\omega_3 > \omega_2$ generate a wave at frequency $\omega_1 = 2\omega_2 - \omega_3$ through the third-order susceptibility $\chi^{(3)}(-\omega_1, \omega_2, \omega_2, -\omega_3)$. The third-order polarization created by such a process is given by (3) and, in the same notation that we used above, the coupled-wave equations that describe the third-order interaction between these three waves are

$$\frac{\partial}{\partial z} A_3^{(a)} = i\chi A_1^{(a)*} \left[A_2^{(a)}\right]^2 e^{-i\Delta k\, z} + i\kappa_3 A_3^{(b)}, \tag{21}$$

$$\frac{\partial}{\partial z} A_2^{(a)} = 2\, i\chi A_1^{(a)} A_2^{(a)*} A_3^{(a)} e^{i\Delta k\, z} + i\kappa_2 A_2^{(b)}, \tag{22}$$

$$\frac{\partial}{\partial z} A_1^{(a)} = i\chi \left[A_2^{(a)}\right]^2 A_3^{(a)*} e^{-i\Delta k\, z} + i\kappa_1 A_1^{(b)}, \tag{23}$$

where $\Delta k = k_3 - 2k_2 + k_1$ is the wave-vector mismatch,

$$\chi = \frac{3}{8} \frac{\chi_{\text{eff}}^{(3)}}{c} \sqrt{\frac{\omega_1 \omega_2^2 \omega_3}{n_1 n_2^2 n_3}}\, S \tag{24}$$

is the effective nonlinear optical coupling constant for this third-order interaction, and S is an overlap integral similar to (9) but involving one additional term. For the process of interest here, the wave at frequency ω_1 is initially zero and grows because of energy transfer from the other two waves. We again assume that the energy in the two pump waves is initially injected in one waveguide, and follow the same procedure outlined earlier for the case of second-order nonlinearities to find the z dependence of the signal wave in the undepleted pump approximation. The two coupled equations for the amplitudes $A_1^{(a)}$ and $A_1^{(b)}$ are

$$\frac{\partial}{\partial z} A_1^{(a)} = \frac{i\chi}{8} e^{-i(2\kappa_2+\kappa_3)z} (e^{i2\kappa_2 z} + 1)^2 (e^{i2\kappa_3 z} + 1) \times e^{-i\Delta k z} A_{2,0}^2 A_{3,0} + i\kappa_1 A_1^{(b)}, \tag{25}$$

$$\frac{\partial}{\partial z} A_1^{(b)} = -\frac{i\chi}{8} e^{-i(2\kappa_2+\kappa_3)z} (e^{i2\kappa_2 z} - 1)^2 (e^{i2\kappa_3 z} - 1) \times e^{-i\Delta k z} A_{2,0}^2 A_{3,0} + i\kappa_1 A_1^{(a)}, \tag{26}$$

where sine and cosine functions have again been expressed in exponential form. The solution for $A_1^{(a)}(z)$ is

$$A_1^{(a)}(z) = \frac{\chi}{8} A_{2,0}^2 A_{3,0}^*\, \xi^{(3)}(z). \tag{27}$$

After substituting (4) and (24) one finds

$$E^{(a,\omega_1)}(z) = \frac{3\chi_{eff}^{(3)} \omega_1}{64 c n_1} \left[E_0^{(a,\omega_2)}\right]^2 \left[E_0^{(a,\omega_3)}\right]^* \xi^{(3)}(z), \tag{28}$$

with

$$\begin{aligned}\xi^{(3)}(z) = {} & \frac{\kappa_1^2 - 2\kappa_2^2 + \kappa_1\kappa_3 + (2\kappa_1 + \kappa_3)\Delta k + \Delta k^2}{K_1 K_3 K_5} 4e^{i\kappa_1 z} \\ & - \frac{\kappa_1^2 - 2\kappa_2^2 + \kappa_1\kappa_3 - (2\kappa_1 + \kappa_3)\Delta k + \Delta k^2}{K_2 K_4 K_6} 4e^{-i\kappa_1 z} \\ & - \frac{2e^{i(\kappa_1 - K_1)z}}{K_1} + \frac{2e^{-i(\kappa_1 - K_2)z}}{K_2} \\ & - \frac{e^{i(\kappa_1 - K_3)z}}{K_3} + \frac{e^{-i(\kappa_1 - K_4)z}}{K_4} \\ & - \frac{e^{i(\kappa_1 - K_5)z}}{K_5} + \frac{e^{-i(\kappa_1 - K_6)z}}{K_6},\end{aligned} \tag{29}$$

and

$$K_1 = \kappa_1 - \kappa_3 + \Delta k, \tag{30}$$

$$K_2 = \kappa_1 - \kappa_3 - \Delta k, \tag{31}$$

$$K_3 = \kappa_1 - 2\kappa_2 + \kappa_3 + \Delta k, \tag{32}$$

$$K_4 = \kappa_1 - 2\kappa_2 + \kappa_3 - \Delta k, \tag{33}$$

$$K_5 = \kappa_1 + 2\kappa_2 + \kappa_3 + \Delta k, \tag{34}$$

$$K_6 = \kappa_1 + 2\kappa_2 + \kappa_3 - \Delta k. \tag{35}$$

Here we see that the third-order interaction can be described with the exact same methodology we followed for the second-order interaction. The CLPM conditions for the third-order interaction are obtained from $K_i = 0, i = 1, \ldots, 6$ as well as a combination of these cases. Again one finds several possibilities. This time, though, the situation is more symmetric and in view of this symmetry it is convenient to collect the above quantities pairwise by defining

$$K_\alpha = \kappa_1 - \kappa_3 \pm \Delta k, \tag{36}$$

$$K_\beta = \kappa_1 - 2\kappa_2 + \kappa_3 \pm \Delta k, \tag{37}$$

$$K_\gamma = \kappa_1 + 2\kappa_2 + \kappa_3 \pm \Delta k. \tag{38}$$

Inspection of Eq. (29) delivers the CLPM conditions summarized in Table III, which are expressed using these quantities. Note that a condition such as $K_\alpha = 0$ means that either $K_1 = 0$ or $K_2 = 0$, but not both. Table III shows that the meaning of all CLPM conditions can be essentially summarized as $\kappa_1 - \kappa_3 = \pm\Delta k$ and $\kappa_1 \pm 2\kappa_2 + \kappa_3 = \pm\Delta k$, which are the cases listed in rows 1–3, corresponding to the conditions when exactly two terms in (29) are dominant. The CLPM conditions in rows 4–6 can all be derived from those in rows 1–3 in special cases where some of the coupling constants are degenerate or equal to zero. Note that adding a third equality in the first column ($K_\alpha = 0, K_\beta = 0, K_\gamma = 0$) does not lead to any more CLPM conditions in addition to those already listed in the table. Also, as was the case for the second-order processes, the condition in row 7 is not a true CLPM condition because it corresponds to conventional exact phase matching in a single waveguide.

Among the CLPM conditions listed in Table III, the one in the first line, involving K_1 or K_2, is the most generally interesting. It is independent of the coupling constant for the ω_2 wave and delivers a steady growth of the amplitude of the signal wave with distance to reach a photon-conversion efficiency of ~100% at an appropriate propagation length (see next section for a discussion of photon-conversion efficiencies). Figure 6 visualizes this situation for the case where $K_2 = 0$. Again, the analytical solution according to (28) and (29) for the undepleted case follows well the exact numerical solution until pump depletion starts becoming significant.

The other primary CLPM conditions (lines 2 and 3 of Table III) depend on all three coupling constants and deliver less signal intensity. The degenerate limiting cases for $\kappa_3 = \kappa_2 = 0$ or $\kappa_1 = \kappa_2 = 0$ given in row 5 deliver the best efficiencies. While the case $\kappa_1 = \kappa_2 = 0$ does not appear practically realistic, the one requiring $\kappa_3 = \kappa_2 = 0$ is conceivable. In fact, for a large difference in wavelength between short-wavelength pump waves at ω_3 and ω_2 and long-wavelength signal wave at ω_1 one could achieve the limit $\kappa_1 \gg \kappa_2, \kappa_3$, which may make the coupling length for the two short-wavelength pump waves longer than the waveguide length necessary to generate sufficient signal power. Finally, we note that the only solution for this example where the generated wave oscillates between the waveguides is the one for the second case of row 4 in Table III. However, also in this case the related CLPM condition is unlikely to be realized in practice as it requires the equality of the coupling constants for two potentially rather distant wavelengths.

III. ADDITIONAL DISCUSSION

In addition to the derivations of CLPM conditions and effective nonlinearity that we presented in the previous sections, the nature of the CLPM process also necessitates a deeper discussion of the ultimate efficiency of the nonlinear optical frequency conversion at longer propagation lengths, for which pump depletion occurs. This is important because a full analysis based on the coupled-wave equations [Eqs. (5)–(7)] in the two parallel waveguides shows that not all CLPM conditions allow one to reach the maximum possible conversion efficiency just by increasing the interaction length. As an example, consider the SFG process shown in Fig. 2: The two pump waves clearly trend towards a situation where half of

TABLE III. CLPM conditions for a third-order interaction generating a wave $\omega_1 = 2\omega_2 - \omega_3$ in two coupled waveguides. The maximum photon-conversion efficiency $\eta^{(3)}_{\max}$ in the depleted regime is also given.

	CLPM rule	Effective condition	$\lim_{z\to\infty}[\xi^{(3)}/z]$	$\eta^{(3)}_{\max}(\%)$
1	$K_\alpha = 0$	$\mp\Delta k = \kappa_1 - \kappa_3$	$2ie^{\pm i\kappa_1 z}$	~100
2	$K_\beta = 0$	$\mp\Delta k = \kappa_1 - 2\kappa_2 + \kappa_3$	$ie^{\pm i\kappa_1 z}$	~50
3	$K_\gamma = 0$	$\mp\Delta k = \kappa_1 + 2\kappa_2 + \kappa_3$	$ie^{\pm i\kappa_1 z}$	~50
4	$K_\alpha = K_\beta = 0$	$\pm\Delta k = -\kappa_1 + \kappa_2, \kappa_2 = \kappa_3$ $\pm\Delta k = \kappa_2 - \kappa_3, \kappa_1 = \kappa_2$	$3ie^{\pm i\kappa_1 z}$ $ie^{\mp i\kappa_1 z} + 2i\cos(\kappa_1 z)$	~80 ~86
5	$K_\alpha = K_\gamma = 0$	$\pm\Delta k = \kappa_1, \kappa_2 = \kappa_3 = 0$ $\pm\Delta k = \kappa_3, \kappa_1 = \kappa_2 = 0$	$4ie^{\mp i\kappa_1 z}$ $4i$	~100 ~100
6	$K_\beta = K_\gamma = 0$	$\pm\Delta k = \kappa_1 + \kappa_3, \kappa_2 = 0$ $\pm\Delta k = 2\kappa_2, \kappa_1 = \kappa_3 = 0$	$2ie^{\mp i\kappa_1 z}$ $2i$	~100 ~50
7	Several	$\Delta k = \kappa_1 = \kappa_2 = \kappa_3 = 0$	$8i$	100

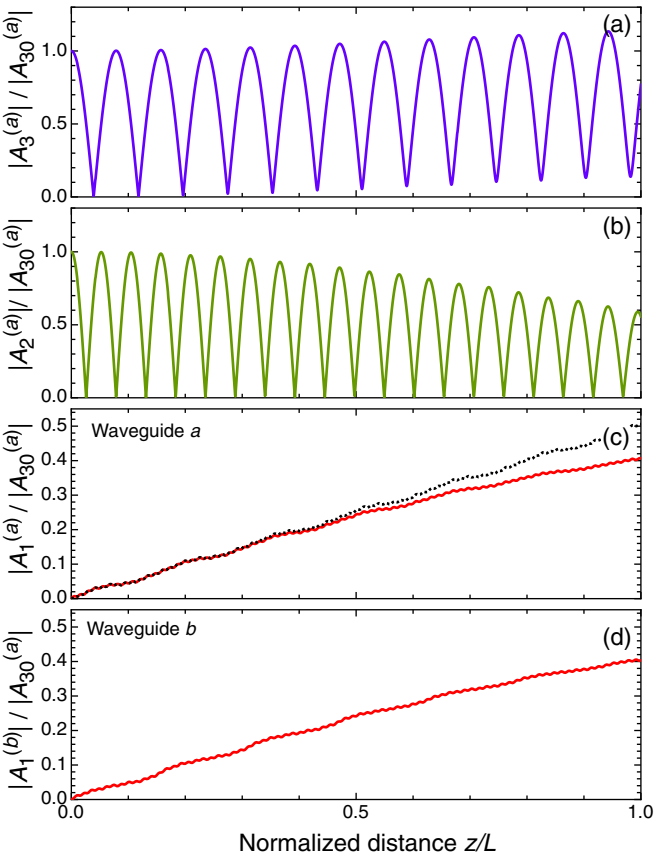

FIG. 6. (Color online) Spatial evolution of the amplitudes of the interacting waves for third-order frequency down-conversion, $\omega_1 = 2\omega_2 - \omega_3$ under CLPM condition $K_2 = 0$ (row 1 in Table III) in parallel waveguides of length L. Panels (a) and (b) give the amplitudes, in waveguide a, of the pump waves at frequency ω_3 and ω_2, respectively. The generated wave amplitude at the frequency ω_1 is shown for both waveguides in (c) and (d), respectively. The solid curves are all in the pump depletion regime. The black dotted curve in (c) corresponds to the analytical solution from (28) and (29) in the undepleted regime. For these plots $\tilde{A} \equiv (|A_{3,0}^{(a)}||A_{2,0}^{(a)}|^2)^{1/3}$, $\Delta kL = 200$, $\kappa_1 L = 240$, $\kappa_2 L = 60$, $\kappa_3 L = 40$, and $L\chi\tilde{A}^2 = 2$. The curves are normalized to the initial amplitude of the wave ω_3 injected in waveguide a.

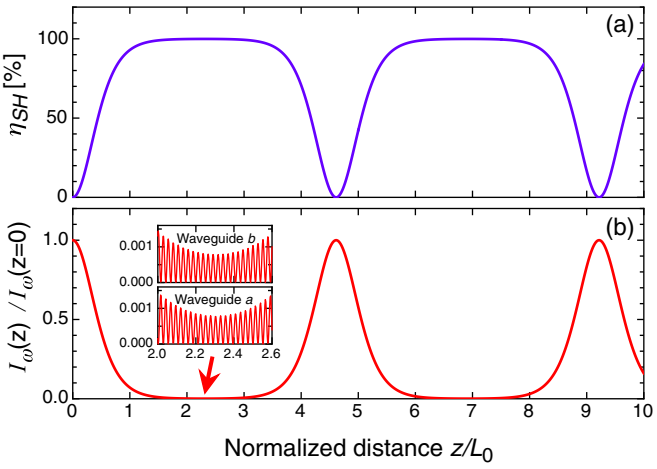

FIG. 7. (Color online) Periodic behavior of second-harmonic generation in the pump depletion regime. (a) Dependence of the photon-conversion efficiency η^{SH} on propagation distance under the CLPM condition in the first line of Table II ($\Delta k = \kappa_3$). (b) Evolution of the corresponding total normalized pump wave photon intensity, where $I_\omega(z) \propto |A_1^{(a)}(z)|^2 + |A_1^{(b)}(z)|^2$ and $I_\omega(z=0) \propto |A_1^{(a)}(0)|^2$. The inset in (b) shows the photon intensity of the fundamental wave in each individual waveguide around the point of maximum pump depletion. The parameters are as in Fig. 4, $\Delta kL_0 = \kappa_3 L_0 = 40$, $\kappa_1 L_0 = 120$, and $L_0 d = 2/|A_{1,0}^{(a)}|$.

each normalized amplitude (one-quarter of the initial number of photons) is left in each one of the two waveguides. At this point, only 50% of the initial number of photons is in the sum-frequency wave, and by extending the calculations to longer propagation lengths we have seen that after this ∼50% conversion state is reached, further propagation leads to the full re-creation of the two pump waves accompanied by the depletion of the generated sum-frequency wave. This imposes a maximum of ∼50% on the photon-conversion efficiency of this process, a maximum that is not apparent from the CLPM solution in the nondepleted wave approximation. In this section we present the definitions of photon-conversion efficiency that we reported in the previous tables, and discuss the maximum efficiencies that can be reached in every CLPM configuration.

It is useful to first discuss the case of SHG. In an ideal case of conventional phase matching in a single waveguide, obtained, for example, using birefringence or the modulation of the nonlinearity, the classical theory for SHG predicts that 100% conversion efficiency is approached asymptotically with propagation length following a $\tanh^2$ functional form [1,12] and that ultimately only the second harmonic wave remains. This corresponds to a photon-conversion efficiency $\eta_{\mathrm{SH}} = 100\%$. In addition, the classical theory does not predict any nonlinear back-conversion to the fundamental frequency after this state has been reached, because the direction of energy flow between the two interacting waves is determined only by their respective phase shifts, which do not change during propagation.

Figure 7 shows the propagation length dependence of the photon-conversion efficiency, η^{SH}, for SHG in parallel waveguides using the first CLPM case listed in Table II. In this case, η^{SH} reaches essentially 100%, like in the case of an individual uncoupled waveguide, or bulk crystal under perfect phase matching, but a small portion of the fundamental wave is left over. As propagation continues, the fundamental wave is recreated again in full, depleting the SH wave back to zero, and then the process starts again, creating the periodic behavior shown in the figure, which is not predicted for standard phase-matched SHG. It is interesting to note that the oscillations observed for CLPM in coupled waveguides are similar—even though they have a completely different origin—to the behavior predicted by a quantum mechanical analysis of SHG [14], where vacuum fluctuations and spontaneous emission processes produce an accumulated phase shift between the interacting waves that ultimately leads to the reversal of the direction of energy flow between the two waves.

The periodic modulation of the frequency conversion efficiency observed in the CLPM case [Fig. 7(a)] is due to the fact that CLPM phase matching is achieved by compensating

the phase differences accumulated during propagation in a waveguide with the phase differences accumulated because of the fields oscillating between the two waveguides, which makes the process also dependent on the distribution of field amplitudes between the two waveguides. While the analytical results we presented earlier show that the CLPM conditions correspond to complete phase matching, pump depletion can lead to a power distribution between the two waveguides that does not support further conversion. Often, this state is characterized by a pump wave becoming equally distributed between the two waveguides. For the SHG example discussed above, this has a negligible effect on the maximum photon-conversion efficiency; but when the maximal $\eta^{\mathrm{SH}} \sim 100\%$ is reached, there is still a small remnant fundamental wave amplitude oscillating between the two waveguides. With further propagation, this remnant wave then seeds a reverse conversion process $2\omega - \omega \rightarrow \omega$, which is also phase matched and is described by the same CLPM condition and coupled wave equations that lead to SHG conversion in the first place. The (phase-matched) reverse process then "explodes," recreating the fundamental with almost 100% efficiency, and the whole cycle repeats.

We find that all the CLPM phase-matching processes studied in this work exhibit a periodic modulation of the photon-conversion efficiency in the depleted pump regime; in some cases the maximum efficiency observed is very close to the ideal case for a given nonlinear optical process, in some other cases it is not. To characterize the effectiveness of the CLPM process we defined a photon-conversion efficiency for all frequency conversion processes we considered. In all cases, our initial condition was the practically interesting one of all pump waves injected in one of the two waveguides, with the generated wave starting at zero amplitude. We defined the photon-conversion efficiencies as the number of photons created in the generated wave (summing those found in each waveguide) divided by the number of photons ideally expected for 100% conversion in each nonlinear process. The maximum photon-conversion efficiencies for SHG ($\eta^{\mathrm{SH}}_{\mathrm{max}}$), SFG ($\eta^{\mathrm{SF}}_{\mathrm{max}}$), DFG ($\eta^{\mathrm{DF}}_{\mathrm{max}}$), and for third-order frequency down-conversion ($\eta^{(3)}_{\mathrm{max}}$), are given for each CLPM condition in Tables I–III. In some cases, an effective conversion efficiency of nearly 100% is reached, similar to the case of SHG discussed above; in other cases the maximum conversion efficiency is limited to ∼50%. Tables I–III show that for every one of the CLPM conversion processes one can reach at least 50% photon-conversion efficiency and that at least one CLPM condition with nearly 100% conversion exists for each type of nonlinear interaction.

We mentioned one example when the maximum conversion efficiency is 50% at the beginning of this section: It is the SFG case presented in Fig. 2, where the maximum conversion state is characterized by half of the fundamental photons being distributed equally between the two waveguides and is followed by a return to the initial condition and a subsequent periodic modulation with propagation distance. The same behavior is observed for all of the CLPM conditions in the first four rows of Table I. The period of the oscillation in conversion efficiency is similar for all cases, and depends essentially only on the effective nonlinearity, varying little with the value of the coupling constants. Another example is DFG, also using any of the CLPM conditions in the first four rows of Table I. In DFG, a pump photon at ω_3 is annihilated to create a photon at ω_2 and one at the difference frequency ω_1. A DFG process reaches 100% photon-conversion efficiency once the pump at ω_3 has been fully depleted (and the pump at ω_2 has been correspondingly amplified). This is possible for DFG using the CLPM condition in row 5 of Table I, a case that we depicted in Fig. 5. But for the CLPM conditions in the first four rows of Table I, the pump wave at ω_3 can only be depleted down to half its initial amplitude in each waveguide. This corresponds to half the initial number of photons at ω_3 still surviving, equally distributed between the two waveguides, giving a maximum photon-conversion efficiency of 50%. From this analysis we can in general say that for some CLPM conditions half the photons from a pump wave get "trapped" in an equidistributed state between the two waveguides, and cannot be converted anymore. Once this situation with equal pump power in both waveguides has been reached, the direction of energy flow changes sign, causing the pump power to "rebound" (going back to the initial state of full oscillation between the two waveguides) while the generated wave is depleted again.

The cases where the maximum conversion efficiency has been given as ∼86%, ∼80% or ∼98% are in general characterized by a complex spatial dynamics, and the photon-conversion efficiencies provided in the tables are the value observed for the first maximum in conversion efficiency. For instance, for all cases with $\eta_{\mathrm{max}} \sim 86\%$ there is a spatially transient maximum of the conversion efficiency, followed by a damped oscillation towards a quasi-steady-state with ∼50% efficiency, all this being followed by the reversed conversion process that finally makes the evolution of the amplitudes with propagation length, as in general expected for CLPM, periodic.

We conclude this section with a note on what we think are the most promising situations in which CLPM schemes could be effectively employed.

The second-order CLPM processes seem particularly attractive for frequency conversion applications in isotropic materials that possess large optical nonlinearities, but for which birefringent phase matching cannot be applied and conventional quasi-phase-matching methods are difficult. As an example we mention gallium arsenide (GaAs), which has a large nonlinearity and a wide transparency range, making it very attractive for mid-IR coherent sources (e.g., with generated wavelengths in the atmospheric transmission windows). While relevant efforts to engineer quasi-phase-matching in GaAs have been ongoing—starting from diffusion bonding of periodically orientation-reversed thin wafers [15] and more recently followed by directly grown orientation-patterned crystals [16–20]—the use of the CLPM processes discussed in this work represents a valid alternative that can be easily realized by simply creating two parallel waveguides using well-established methods. CLPM would then enable, e.g., difference-frequency generation between wavelengths of 1.5 and 2.1 μm to deliver radiation near 5.25 μm, while a source at ∼10 μm could be built by difference-frequency generation between 2.5 μm and 2 μm. For GaAs, this last example is associated with a phase mismatch of the order of $\Delta k \approx 75\ \mathrm{mm}^{-1}$, for which one can achieve CLPM in parallel waveguides by, e.g., a $K_2 = 0$ process using coupling constants of the same order of magnitude. Such values are well under reach for waveguides based on GaAs/AlGaAs technology

[10]. Another intriguing possibility is that of designing two waveguides that are not exactly parallel, so that the coupling coefficients, and therefore the wavelength at which CLPM is achieved, vary over the length of the waveguides. This may lead to a wavelength converter that, working over large bandwidths, can support tunable laser sources.

The third-order DFG process we presented could be naturally implemented in dual-core fibers. Microstructured and photonic bandgap fibers also offer an attractive playground both for controlling the optical modes at different wavelengths and for tuning the coupling constants between the cores, while at the same time providing large interaction lengths. Depending on the application, silica fibers as well as chalcogenide fibers or other oxide fibers could be used. Again, no periodic modulation of the fiber properties are required to implement CLPM; it is sufficient to design two appropriately spaced cores. Then, depending on the transparency range of the fiber material it would be possible to use the $2\omega_2 - \omega_3 \rightarrow \omega_1$ CLPM process to combine two near-infrared laser sources to obtain longer wavelength radiation. As an example, mixing the outputs of a 1550-nm fiber laser and of a 1064-nm Nd:YAG laser would deliver radiation near 2.85 μm, or combining the output of a 960-nm laser diode that pumps an erbium fiber laser with the output of the fiber laser itself would produce a wavelength of 4 μm. Further in the infrared, mixing of 2.1 μm and 1.2 or 1.3 μm would deliver a source at 8.4 or 5.5 μm, and so on.

IV. CONCLUSIONS

We presented an in-depth discussion of how it is possible to obtain an effective quasi-phase-matched nonlinear optical three-wave interaction process in two parallel, coupled waveguides without any spatial modulation of linear or nonlinear optical properties along the propagation length. We called this effect coupling-length phase matching and demonstrated that it works for any second-order nonlinear optical interaction, from second harmonic generation to parametric processes, and also for third-order nonlinear optical interactions. We derived all the CLPM conditions for second-order nonlinear optical frequency conversion and for third-order difference-frequency generation based on a $2\omega_2 - \omega_3 \rightarrow \omega_1$ process, and we determined the effective optical nonlinearity for all of them, as well as the corresponding maximum photon-conversion efficiency, which was found to vary between 50% and 100%, depending on the CLPM configuration.

[1] J. A. Armstrong, N. Bloembergen, J. Ducuing, and P. S. Pershan, Phys. Rev. **127**, 1918 (1962).

[2] M. M. Fejer, G. A. Magel, D. H. Jundt, and R. L. Byer, IEEE J. Quantum Electron. **28**, 2631 (1992).

[3] J. B. Driscoll, N. Ophir, R. R. Grote, J. I. Dadap, N. C. Panoiu, K. Bergman, and R. M. Osgood, Opt. Express **20**, 9227 (2012).

[4] S. Richard, J. Opt. Soc. Am. B **27**, 1504 (2010).

[5] I. Christov, H. Kapteyn, and M. Murnane, Opt. Express **7**, 362 (2000).

[6] A. Paul, R. A. Bartels, R. Tobey, H. Green, S. Weiman, I. P. Christov, M. M. Murnane, H. C. Kapteyn, and S. Backus, Nature (London) **421**, 51 (2003).

[7] A. A. Maier, Sov. J. Quantum Electr. **10**, 925 (1980).

[8] X. G. Huang and M. R. Wang, Opt. Commun. **150**, 235 (1998).

[9] P. Dong and A. G. Kirk, Phys. Rev. Lett. **93**, 133901 (2004).

[10] P. Dong, J. Upham, A. Jugessur, and A. G. Kirk, Opt. Express **14**, 2256 (2006).

[11] K. Koynov, S. M. Saltiel, and Y. S. Kivshar, Opt. Lett. **30**, 2284 (2005).

[12] P. N. Butcher and D. Cotter, *The Elements of Nonlinear Optics* (Cambridge University Press, Cambridge, 1991).

[13] W.-P. Huang, J. Opt. Soc. Am. A **11**, 963 (1994).

[14] D. F. Walls, Phys. Lett. A **32**, 476 (1970).

[15] L. Gordon, G. Woods, R. Eckardt, R. Route, R. Feigelson, M. Fejer, and R. Byer, Elec. Lett. **29**, 1942 (1993).

[16] L. A. Eyres, P. J. Tourreau, T. J. Pinguet, C. B. Ebert, J. S. Harris, M. M. Fejer, L. Becouarn, B. Gerard, and E. Lallier, Appl. Phys. Lett. **79**, 904 (2001).

[17] K. Vodopyanov, O. Levi, P. Kuo, T. Pinguet, J. Harris, M. Fejer, B. Gerard, L. Becouarn, and E. Lallier, Opt. Lett. **29**, 1912 (2004).

[18] A. Grisard, E. Lallier, and B. Gérard, Opt. Mater. Express **2**, 1020 (2012).

[19] C. R. Phillips, J. Jiang, C. Mohr, A. C. Lin, C. Langrock, M. Snure, D. Bliss, M. Zhu, I. Hartl, J. S. Harris, M. E. Fermann, and M. M. Fejer, Opt. Lett. **37**, 2928 (2012).

[20] L. P. Gonzalez, D. C. Upchurch, P. G. Schunemann, L. Mohnkern, and S. Guha, Opt. Lett. **38**, 320 (2013).